Measurement report: Simultaneous measurement on gas- and particle-phase water-soluble organics in Shanghai: Enhanced light absorption of transported Asian dust

Zheng Li[1], Gehui Wang[1,2]*, Binyu Xiao[1], Rongjie Li[1], Can Wu[1,2]*, Shaojun Lv[1], Feng Wu[3], Qingyan Fu[4], Yusen Duan[5]

[1]Key Lab of Geographic Information Science of the Ministry of Education, School of Geographic Sciences, East China Normal University, Shanghai 210062, China

[2]Institute of Eco-Chongming, 20 Cuiniao Rd., Chongming, Shanghai 202150, China

[3]State Key Laboratory of Loess and Quaternary Geology, Institute of Earth Environment, Chinese Academy of Science, Xi'an 710061, China

[4]Key Laboratory of Formation and Prevention of Urban Air Pollution Complex, Ministry of Ecology and Environment, Shanghai Academy of Environmental Sciences, Shanghai, 200233, China

[5]Shanghai Technology Center for Reduction of Pollution and Carbon Emissions, Shanghai, 200233, China

Correspondence to: Prof. Gehui Wang (ghwang@geo.ecnu.edu.cn) and Dr. Can Wu (cwu@geo.ecnu.edu.cn)

25   **Abstract**: To better understand the physicochemical evolution of Asian dust particles during

26   long-range transport, water-soluble organic compounds (WSOCs) in gas- ($WSOC_g$) and

27   particle-phase ($WSOC_p$) in the spring atmosphere of Shanghai during the 2023 dust storm

28   period (DS) and haze events (HE) were simultaneously measured with a 3-h time resolution,

29   and characterized for their optical properties and size distribution. Our results showed that

30   gas-to-particle-phase partitioning coefficients (F_p) of WSOCs in DS (0.30 ± 0.06) was

31   comparable to that in HE (0.32 ± 0.06), although both temperature and relative humidity in

32   DS were not favorable for the partitioning, indicating a promoting role of dust particles in

33   the transformation process of $WSOC_g$ from gas to particle phase. F_p variation was largely

34   driven by aerosol liquid water content in HE but by aerosol acidity in DS. $WSOC_p$ and its

35   light absorption at λ_{365nm} dominated at the fine mode (< 2.1 µm) in non-DS period and the

36   coarse mode (> 2.1 µm) in DS, respectively. Mass absorption coefficient (MAC) of the

37   coarse mode of $WSOC_p$ at λ_{365nm} in DS was 0.8 m^2 g^{-1}, which is four times that (0.20 ± 0.09

38   m^2 g^{-1}) in the source region of Tengger Desert, suggesting a remarkably increase in light

39   absorbing ability of Asian dust during long-range transport. Sharp co-increases of

40   nitroaromatics, imidazoles, and water-soluble organic nitrogen at the coarse mode in the DS

41   period further revealed that such an increasing MAC is mainly caused by adsorption and

42   heterogeneous formation of light absorbing nitrogen-containing organics on the dust surface

43   during long-range transport.

44

1 Introduction

Dust storm (DS) release up to 2 billion tons of dust particles into the global atmosphere annually, exerting significant impacts on visibility, climate, and ecological environment (Li et al., 2014; Tang et al., 2016; Wu et al., 2020; Chen et al., 2023; Ge et al., 2024). During a long range transport physicochemical properties of dust particles can significantly be changed by a series of chemical reactions especially in the downwind region of East Asia, where anthropogenic gas pollutants such as O_3, NO_x and NH_3 are abundant (Wang et al., 2014; Wang et al., 2015; Zhang et al., 2015; Wu et al., 2020; Wang et al., 2025).

Since the majority of oxidation products of atmospheric volatile organic compounds (VOCs) are water-soluble, gas-to-particle-phase partitioning of water-soluble organic compounds (WSOCs) is a major formation pathway of SOA in the atmosphere (Ervens et al., 2011; Liu et al., 2012; Gkatzelis et al., 2021; Lv et al., 2022b; Lv et al., 2022a). The gas-to-particle-phase partitioning process is regulated by a variety of factors such as concentrations of VOCs, NH_3 and NO_x and their compositions, in addition to temperature and relative humidity (RH) (Hennigan et al., 2009; El-Sayed et al., 2018). In the past decade, atmospheric environment in East Asia has changed significantly due to sharp reductions in SO_2 and black carbon (BC) emissions in China, which is currently dominated by NO_x, VOCs and NH_3 along with an increasing level of O_3 (Zhang et al., 2020; Li et al., 2021; Liu et al., 2022; Xiao et al., 2022; Wang et al., 2023; Chen et al., 2024). Dust storm from East Asia desert regions is one of the major contributors to the global atmospheric aerosols (Wang et al., 2020). Such reductions in SO_2 and BC in the East Asia atmospheric environment could also significantly alter the physicochemical evolution process of dust particles during long range transport by adsorption and reactions such as gas-to-particles

partitioning of WSOCs and SOA formation on the dust particle surface. Therefore, field observations on the gas-to-particle-phase partitioning of WSOCs is necessary for better understanding on SOA formation process in the current East Asia atmosphere.

A few studies have indicated that gas-to-particle phase partitioning of WSOCs in China is much more efficient than that in developed countries such as the United States, mainly due to a high level of NH_3 in China (Zhang et al., 2012; Lv et al., 2022b; Lv et al., 2022a). Our recent observation found that such an enhanced gas-to-particle phase partitioning in China not only increase SOA production but also enhance atmospheric aerosol light absorption (Liu et al., 2023). Up to date, most of field investigations on WSOCs partitioning and organic aerosol light absorption have been conducted in winter with a focus on fine particle pollution (Cheng et al., 2016; Yuan et al., 2020; Lv et al., 2022b; Li et al., 2023a; Li et al., 2023b; Liu et al., 2024). In contrast, WSOC partitioning behavior and organic aerosol light absorption in East Asia during spring has rarely been investigated, where dust particles and NH_3 in the troposphere are much more abundant in spring than in winter. In this study we performed a simultaneous measurement on the atmospheric gas- and aerosol-phase WSOCs in Shanghai with a focus on the heterogenous formation of SOA on dust surface and its impact on dust particle optical properties. Our work for the first time unveiled that light absorbing ability of Asian dust is remarkably enhanced during long range transport by formation of light absorbing SOA, which is termed as brown carbon, on dust particle surface.

2 Materials and methods

2.1 Samples collection

The filed observation was conducted from 27 March to 21 April 2023 on the campus of East China Normal University (31.03°, 121.45°), which is situated on the southern area of

93 Shanghai. All instruments were set on the roof of the Atmospheric Observation Station with

94 the air inlet 10 meters above the ground. A modified in-situ gas and aerosol compositions

95 monitor (IGAC, Model 63GA, Fortelice International Co., Ltd., Taiwan, China) was used to

96 synchronously measure gaseous and particulate species with a 3 h interval for WSOCs and a

97 1-h interval for inorganics species and small organic acids, respectively (Lv et al., 2022b; Lv

98 et al., 2022a). For the IGAC sampling system, the air was drawn into a $PM_{2.5}$ cyclone inlet

99 and passed through either a wet rotating denuder (gases) or a steam jet aerosol collector

100 (aerosols). The IGAC monitor is coupled with ICS-5000$^+$ ion chromatography (Thermo) and

101 a TOC/TON analyzer (model TOC/TON-L CPH, Shimadzu, Inc., Japan). Due to the

102 difference in the online instrument detection limits, gas-phase WSOC ($WSOC_g$) and particle

103 phase WSOC ($WSOC_p$) and particle-phase water-soluble organic nitrogen (WSON) were

104 measured with a time resolution of 3 h, while inorganic species organic acids were measured

105 with a time resolution of 1 h. In this study, the concentrations of WSON were calculated as

106 the difference between total nitrogen (TN), which was determined by the online TOC/TON

107 analyzer, and total inorganic nitrogen ($IN = NH_4^+ + NO_2^- + NO_3^-$), which was determined

108 by the IGAC-IC, namely, [WSON] = [TN] −[IN]. The collection efficiency of IGAC system

109 for both gas- and aerosol- phase species is >73% (Lv et al., 2022, 2023).

110 PM$_{2.5}$ filter samples were collected on a day/night basis by using a high-volume

111 sampler (1.13 m^3 min^{-1}, TISCH Environmental, Inc.) in the spring of 2023 from 27 March to

112 21 April 2023 ($N = 50$), while size-segregated aerosols were also collected using an

113 Anderson 9-stage sampler (Thermo Electronic Corporation, USA) at an airflow rate of 28.3

114 L min^{-1} with cutoff points of 0.43, 0.65, 1.1, 2.1, 3.3, 4.7, 5.8 and 9.0 μm, respectively. In

115 this study four sets of the size-resolved aerosol samples were collected with two sets

116 collected in 11-13 April, 2023, which is a dust storm period (DS) (see discussion later),

117   while other two sets of the size-resolved aerosol samples were collected in other non-dust

118   storm periods (NDS) (7-10 April). In addition, PM_{10} samples during a spring dust event of

119   2023 were also collected in Tengger Desert ($N = 3$), which is one of the major dust source

120   regions in East Asia. Field blanks of each types of samples were also collected every 3-5

121   days. All of the filter samples were collected onto the pre-baked (450 °C) quartz filters and

122   stored in a freezer (-18 °C) prior to analysis.

123   Hourly $PM_{2.5}$ and PM_{10} mass concentrations were obtained from the Shanghai

124   Environmental Monitoring Center. The meteorological factors including temperature and

125   RH were monitored by an automatic weather station (MILOS520, Vaisala, Inc., Finland).

126   **2.2 Chemical analysis and light absorption measurement**

127   For the offline-$PM_{2.5}$ samples and 9-stage size-segregated filter samples analysis, a

128   half of each filter sample was cut into pieces and ultrasonically extracted with 45 mL Milli-

129   Q water. The extracts were subsequently filtered with a 0.45 μm syringe filter, and analyzed

130   using ion chromatography (ICS-5000$^+$, Thermo Scientific) for inorganic ions (Na^+, NH_4^+,

131   K^+, Mg^{2+}, Ca^{2+}, Cl^-, NO_2^-, NO_3^-, SO_4^{2-}), organic acids (formic, acetic, oxalic, pyruvic (Pyr)

132   and methanesulfonic acids (MSA). Water-soluble organic (WSOC) and inorganic carbon

133   (WSIC) and WSON of the filter samples were determined by the TOC/TON analyzer above.

134   Meanwhile, optical absorptions of WSOC, i.e., water-soluble brown carbon (BrC), in the

135   size-resolved samples were measured using a liquid waveguide capillary cell UV–Vis

136   spectrometer (LWCC, World Precision Instrument, Inc., USA) coupled with a long effective

137   path length. In our application, light from a light source (DH-Mini, Ocean Optics, Inc.,

138   USA) is introduced into the LWCC through a fiber optic cable and, after passing through the

139   LWCC, is collected to the detector (Ocean Optics, Inc., USA). Each instrument was

140   calibrated weekly using authentic standards containing the target compounds. The detection

141 limits of TC, IC and TN were 0.04, 0.05 and 0.01 mg/L, and other species detection limits

142 were less than 0.01 ml/L.

143   Nitroaromatics (NACs) in the filter samples were extracted by a mixture of methanol

144 and dichloromethane (2:1, v:v), derivatized with N,O-bis-(trimethylsilyl)trifluoroacetamide

145 (BSTFA) and quantified by a gas chromatography (GC, HP7890B) coupled with mass

146 spectroscopy (MS, HP5977B) (Wang et al., 2009). In this study, four NACs were

147 determined, which are 4-nitrophenol (4NP), 2-methoxy-4-nitrophenol (4NGA), 2-methoxy-

148 5-nitrophenol (5NGA), and 5-nitrosalicylicylic acid (5NSA), respectively. For imidiazoles

149 (IMS), an aliquot of the filter samples was extracted with 5 mL of ultrapure water with 1%

150 (v/v) methanol and analyzed using high-performance liquid chromatography (HPLC,

151 Thermo Scientific) coupled with orbitrap-mass spectrometry (MS, Thermo Scientific). A

152 total of eight imidazole compounds (IMs) were quantified in this study, which are 2-

153 mechtlimidazole (2MI), 4(5)-methylimidazole (4MI), 1-ethylimidazole (1EI), 2-

154 ethylimidazole (2EI), 1-phenylimidazole (1PhI), 2-phenylimidazole (2PhI), 2-

155 imidazolcarboxaldehyde (2IC) and 4-imidazolcarboxaldehyde (4IC), respectively.

156 Recoveries of all the detected compounds were better than 85%. The detailed method for the

157 organic aerosol analysis can be found elsewhere (Li et al., 2020; Li et al., 2023a; Liu et al.,

158 2023).

159 **2.3 Calculations on ALWC and pH of PM$_{2.5}$**

160   ALWC and pH were estimated using the thermodynamic model ISORROPIA-II, based

161 on the hourly measured NH$_3$, RH, T and PM$_{2.5}$-related chemical compounds. A forward

162 metastable mode was chosen for the calculation (Fountoukis and Nenes, 2007; Song et al.,

163 2018; Wang et al., 2018). Figure S1 compares the concentrations of NH$_3$ and NO$_3^-$ measured

164 by the IGAC instrument with those predicted by ISORROPIA-II model. As shown in Figure

165   S1, the predicted are very close to the measured, suggesting that the metastable mode we

166   used can remarkably reproduce the measured and the model results including ALWC and

167   acidity (pH) are reliable. It should be noted that the samples collected under RH > 95%

168   conditions were excluded in this study, because RH > 95% conditions could increase ALWC

169   and pH estimation uncertainties.

3 Results and discussion

3.1 Chemical characteristics of different aerosol pollution events

172   During the campaign $PM_{2.5}$ varied from 3.0 to 87 µg m^{-3} with an average of 30 ± 14

173   µg m^{-3} (Figure 1 and Table 1), which is slightly lower than the National Air Quality I Grade

174   Standard of China (35 µg m^{-3}). However, particle pollution with a daily $PM_{2.5}$ > 35 µg m^{-3}

175   were frequently observed during the campaign (Figure 1). In this study, a pollution event

176   lasting for more than two consecutive days with a daily $PM_{2.5}$ levels > 35 µg m^{-3} was

177   defined as a haze episode. As shown in Figure 1, a dust storm event had occurred in

178   Shanghai from 11 to 13 April with a PM_{10} concentration sharply increased to 986 µg m^{-3},

179   resulting in the $PM_{2.5}/PM_{10}$ mass ratio down to less than 0.1 and Ca^{2+} up to 2.5 µg m^{-3}

180   (Table 1 and Figure 1). Thus, here we classified the observation periods of 5-9, 11-13, April

181   as a haze event (HE) and dust storm event (DS), respectively. While those periods with a

182   daily $PM_{2.5}$ < 35 µg m^{-3} was defined as a clean period (CP), which occurred from 18-22,

183   April (Figure 1).

184   As seen in Table 1, secondary ions (sulfate, nitrate, ammonium, SNA) were the

185   dominant species among the detected components. The mass contribution of SNA to $PM_{2.5}$

186   reached up to ~69 % in HE, which was 1.6-fold of that in CP, indicating a key role of SNA

187   in the haze formation process. During the DS period, SNA loadings in Shanghai were

188   comparable to that in CP, which only accounted for ~17 % of $PM_{2.5}$. However, the

189 proportion is still remarkably higher than those in Asian desert sources and upwind cities

190 (Table S1), indicating a significant formation of SNA during the dust long-transport (t test,

191 $p<0.01$). Ca^{2+}, Na^+ and Mg^{2+} were 4–8 times higher in DS than in HE. Such enhancements

192 in metal cations affected the aerosol acidity, resulting in the pH of fine particles ($PM_{2.5}$)

193 rising from 3.3 in non-dust storm period (NDS) to 7.5 in DS (Figure 1c).

194 As shown in Table 1, there was a large variability in $WSOC_g$ concentration, which

195 ranged from 0.7 to 19.6 $\mu gC\ m^{-3}$ with an average loading of $8.2 \pm 3.3\ \mu gC\ m^{-3}$ in the CP

196 period and was higher than those in the HE and DS periods (Table 1). The partitioning

197 coefficient of WSOC ($F_p = WSOC_p / (WSOC_p + WSOC_g)$) ($0.32 \pm 0.06$, Table1) in HE was

198 33% higher than that in CP (0.24 ± 0.06, Table1) and robustly correlated with $WSOC_p$ ($r =$

199 0.68, $p < 0.01$) (Figure S2a). A similar strong correlation of $PM_{2.5}$ with $WSOC_p$ was also

200 observed in HE but not in DS (Figure S2b). Since most components of SOA are water-

201 soluble, such a strong correlation between F_p and $WSOC_p$ suggests that gas-to-particle-phase

202 partitioning of WSOC is a major formation pathway of SOA in the HE period. WSOC level

203 and F_p in DS (0.3 ± 0.06, Table1) was similar to those in HE and exhibited a well correlation

204 each other ($r = 0.61$, $p < 0.01$) (Figure S2a), indicating that gas-to-particle partitioning of

205 $WSOC_g$ was also an important formation pathway for SOA in the DS period. As seen in

206 Table 1, SNA accounted for $68 \pm 13\%$ $PM_{2.5}$ in HE but only $16 \pm 12\%$ $PM_{2.5}$ in DS, because

207 $PM_{2.5}$ was dominated by secondary species in HE but by mineral components in DS. Thus,

208 unlike the case in HE, there was no correlation between $PM_{2.5}$ and $WSOC_p$ in DS.

209 **3.2 Factors driving WSOC partitioning during aerosol pollution events**

210 As shown in Table 1 and Figure 2a, ALWC in HE was 2.5-fold higher than that in CP

211 period and well correlated with F_p ($r = 0.66$, $p < 0.01$), because $PM_{2.5}$ aerosols in the HE

212 period were enriched in hygroscopic SNA, resulting in a high level of ALWC under the

213   humid conditions (Table 1). Thus, ALWC took a key role controlling the partitioning process

214   of WSOC, similar to the results observed during winter in Shanghai, China and Los Angeles

215   and Atlanta, United States (Hennigan et al., 2009; Zhang et al., 2012; Lv et al., 2022b). In

216   contrast, ALWC in the DS period was almost one order of magnitude lower than that in the

217   HE period (Table 1) and did not correlate with F_p (Figure 2a), because SNA concentrations

218   in the DS period were much lower than those in the HE period (Table 1). Moreover, RH in

219   the DS period was $44 \pm 18\%$ (Table1), which is higher than the efflorescence RH of SNA

220   but lower than their deliquescence RH and thus not favorable for the formation of aerosol

221   liquid water (Wang et al., 2016, 2025). Therefore, WSOC partitioning process during the DS

222   was not regulated by ALWC. In this study, we calculated the contributions of organic matter

223   (OM) and water-soluble inorganic ions to ALWC in the HE period. It can be seen from

224   Figure S3a, NH_4NO_3 was the largest contributor to ALWC during the haze pollution period,

225   followed by $(NH_4)_2SO_4$ and OM, with the contributions being $56.4 \pm 12.2\%$, $29.1 \pm 7.1\%$,

226   and $6.1 \pm 3.8\%$, respectively. Figure 2b shows that ALWC increased exponentially along

227   with the NH_3-partitioning coefficient ($\varepsilon(NH_4^+) = NH_4^+ / (NH_3 + NH_4^+)$) in the HE period and

228    $WSOC_p$ increased in tandem with an increas in ALWC in HE, which increased along with

229   TNH_x concentrations (Figure 2c). Moreover, as seen in Figure 2d, $WSOC_p$ well correlated

230   with TNH_x ($= NH_3 + NH_4^+$) in HE ($r =0.72$, $p < 0.01$), indicating that abundant ammonia in

231   the atmosphere of Shanghai is favorable for WSOC partitioning and SOA formation. Na et

232   al., (2007) and Liu et al., (2021) reported that NH_3 can be neutralized with organic acids to

233   form ammonium salts, thus induce rapid increase in SOA yields. It can be seen from Figure

234   S3b that particulate carboxylates exponentially increased along with an increase of TNH_x

235   concentration, further demonstrating that NH_3 neutralization with organic acids was also

236   responsible for the strong correlations of TNH_x with F_p in the HE period.
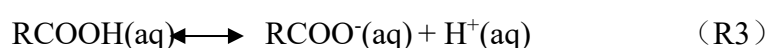
237   During the DS period, F_p of WSOCs robustly correlated with pH ($r = 0.98$, $p < 0.01$,

238   Figure 2e), suggesting that pH was a key factor controlling the WSOC partitioning. As we

239   discussed before, ammonia played an important role in $WSOC_p$ formation during the HE

240   period with a strong correlation with TNH_x in HE (Figure 2d). However, such a correlation

241   was not observed in DS (Figure 2d), which indicates that ammonia was not an effective factor

242   driving the WSOC partitioning process in the DS period. As shown in Figure 2f, the sum of

243   Ca^{2+}, Na^+ and Mg^{2+} concentrations showed a significantly correlation with particulate organic

244   acids ($r = 0.88$, $p < 0.01$), including formic, acetic and oxalic acids, during the DS period,

245   because the lower acidity of aerosols in the DS period was favorable for the reactive uptake

246   of acidic organics by dust surface (Table S2).

247   To further analyze the factors controlling the WSOC partitioning, we investigated the

248   partitioning process of formic and acetic acids, which are abundant species of WSOCs in the

249   atmosphere (Table S2). As shown in Figure S4, F_p of formic and acetic acids in HE

250   presented strong correlations with ALWC, pH and T. In DS, however, compared with

251   ALWC and T, F_p of formic and acetic acids exhibited a stronger correlation with pH, further

252   indicating that the partitioning of WSOC was more significantly affected by the particle

253   acidity in the presence of dust storm.

254   Apart from the above factors that influence the F_p variations, aerosol mass loading may

255   also affect the partitioning of organic species (Pankow, 1994; Lutz et al., 2019). According

256   to the Raoult's law, the field gas-particle partitioning coefficient can be described as follows

257   (Pankow, 1994):

258
$$K_i = \frac{i_{particle}}{i_{gas}TSP} \qquad (R1)$$

259   where K_i is the partitioning constant of i compound, $i_{particle/gas}$ are the particle and gas

260   phase concentrations of compound i (formic and acetic acids in PM$_{2.5}$ are chosen here), and

261   *TSP* is the concentration of total suspended particulate material (PM$_{2.5}$ are used here). Figure

262   S5 presents the $i_{particle}/i_{gas}$ ratios versus PM$_{2.5}$ for formic and acetic acids during HE and DS

263   periods. Particle/gas ratios of formic and acetic acids did not correlate with PM$_{2.5}$ in both HE

264   and DS periods, indicating that the effect of aerosol mass loading on the uptake of organic

265   acids during the campaign was not significant. As shown in Table 1, the PM$_{2.5}$ loadings in

266   DS were comparable to those in HE, although PM$_{10}$ loading was much higher in the dust

267   storm period. Moreover, the pH (4.8 ± 1.5, Table 1) of PM$_{2.5}$ in DS was 1.4 units higher than

268   that (3.4 ± 0.3) in HE, which means that H$^+$ concentration in DS was one order of magnitude

269   lower than that in HE. According to the equations R2 and R3, the low H$^+$ concentration in

270   DS period was favorable for the organic acid equilibria shifting toward the aerosol aqueous

271   phase. Thus, the impact of pH variation on F_p was much more significant than PM aerosol

272   mass loading in DS, taking a key role in WSOC partitioning process during the DS event.

273         $$RCOOH(g) \longleftrightarrow RCOOH(aq) \qquad （R2）$$
274         $$RCOOH(aq) \longleftrightarrow RCOO^-(aq) + H^+(aq) \qquad （R3）$$

3.3 Gas-to-particle partitioning of WSOC on size-resolved particles

276   Figure 3 shows the size distributions of water-soluble organic species, including

277   WSOC$_p$, NACs, IMs and WSON$_p$, in the non-dust storm (NDS) and dust storm (DS) periods

278   in Shanghai during the campaign. As shown in Figure 3a, WSOC$_p$ showed a bimodal size

279   distribution pattern in both periods. The relative abundance of WSOC$_p$ in the coarse mode (>

280   2.1 μm) accounted for 59 % of the total during the DS period, which is 25 % higher than that

281   in the NDS period. Oxalic, pyruvic and methanesulfonic acids are typical SOA tracers in the

282   atmosphere (Wang et al., 2012; Huang et al., 2014; Wang et al., 2015; Wang et al., 2016;

283   Tang et al., 2019), which displayed a bimodal pattern in the NDS period with two peaks

284   distributing in the fine and coarse modes, respectively (Figure S6). In contrast, those

285   secondary SOA presented a monomodal size distribution pattern in the DS period with a

286   predominant peak in the coarse mode only. As seen in Table 2, their concentrations are

287   substantially higher than those in the Tengger Desert region and mostly stayed in the coarse

288   mode (> 2.1μm) during the DS period, clearly revealing an enhanced SOA formation on the

289   dust particles during their transport from the Asian desert source region to the downwind

290   city. As shown in Figure S7, F_p of WSOC in the fine and coarse modes were larger than

291   those in the NDS period, especially for the coarse mode of F_p, which was 60 % higher in the

292   DS period than that in the NDS period, indicating that dust surface is favorable for the

293   uptake of $WSOC_g$.

294   Previous studies reported that NACs can be formed secondarily via both gas-phase and

295   aqueous-phase reaction pathways (Wang et al., 2019; Hems et al., 2020; Ren et al., 2023).

296   For example, benzene reacts with OH radicals and generates phenol. Then, phenol further

297   reacts with NO_2 and yields gaseous nitrophenol (Liang et al., 2020). The latter subsequently

298   partitions to the condensed phase (Lauraguais et al., 2014). Moreover, phenol and catechol

299   can also react with NO_2 radical in the aerosol aqueous phase to form the corresponding

300   NACs (Vione et al., 2004). Our recent study in Shanghai found that the gaseous NACs (i.e.,

301   nitrophenol and methylnitrophenols) concentrations were 2 orders of magnitude higher than

302   the particulate ones (Liu et al., 2023). As seen in Figure 3b, NACs showed a bimodal pattern

303   with a relatively larger peak in the coarse mode during the NDS period. In contrast, NACs

304   almost entirely stayed in the coarse mode during the DS event. Such distinct size distribution

305   patterns indicate that NACs in Shanghai in the DS event were mainly formed by a gas-phase

306   oxidation and subsequent partitioning onto the dust surface.

307   IMs can be directly emitted from biomass burning process and secondarily produced

308   from reactions of carbonyls with amines and ammonia in aerosol aqueous phase (Lian et al.,

309   2021; Liu et al., 2023). As shown in Figure 3c, IMs predominantly stayed in the fine mode

310   in the NDS period. However, in the DS period IMs showed a bimodal pattern in the DS

311   period with two equivalent peaks in the fine and coarse modes. respectively. Since IMs were

312   not detected in the Desert source samples (Table 2), the peak of IMs in the coarse particles in

313   Shanghai during the DS period are expected to be secondarily formed on the dust particles

314   via heterogeneous reactions such as the reactions of glyoxal and methylglyoxal with free

315   NH_3 molecules in aerosol aqueous phase (Liu et al., 2023). Size-resolved chemistry analysis

316   results showed that NO_3^- in the coarse mode poorly correlated with NH_4^+ (> 2.1 μm) in the

317   NDS period ($r = 0.29$, $p < 0.05$) but robustly correlated with NH_4^+ ($r = 0.76$, $p < 0.01$) in the

318   DS period (Figure S8a). Field observations found that NO_3^- in the coarse mode during the

319   NDS period is formed via reaction uptake of gaseous HNO_3 by coarse particles and exists

320   mostly as $Ca(NO_3)_2$ (Tobo et al., 2010; Wu et al., 2020). Therefore, NO_3^- in coarse particles

321   poorly correlates with NH_4^+ (Figure S8a), because coarse particles are usually enriched with

322    $CaCO_3$, which is more basic than NH_3 (Laskin et al., 2005; Li and Shao, 2009; Tobo et al.,

323   2010). However, in a typical Asian dust storm period the coarse mode of NO_3^- usually

324   strongly correlates with NH_4^+, because there are large amounts of mineral dust particles in

325   Asian dessert region such as Na_2SO_4, $CaSO_4$ and $NaCl$ (Wu et al., 2020). Those mineral dust

326   particles are hygroscopic and can promote the hydrolysis of N_2O_5 on dust particle surface

327   and produce HNO_3, which subsequently neutralize with NH_3 as NH_4NO_3 (Wang et al., 2014;

328   Wu et al., 2020). Therefore, a linear correlation between NO_3^- and NH_4^+ in the coarse mode

329   was observed in Shanghai in DS during the campaign (Figure S8a). As we discussed in

330   section 3.2, NH_4NO_3 was the biggest contributor to ALWC. Therefore, the formation of

331   hygroscopic species such as NH_4NO_3 can enhance gas-to-particle phase partitioning of

332    $WSOC_g$ and the heterogeneous reactions on the dust surface. Similarly, the coarse mode of

333   oxalic acid robustly and linearly correlated with NH_4^+ in the DS period but not correlated

334   with NH_4^+ in the NDS period ($r = 0.97$, $p < 0.01$) (Figure S8b), which again suggests an

335   enhanced heterogeneous reaction of SOA on the mineral particle surface during Asian dust

336   long-range transport.

337   **3.4 Enhanced light absorption ability of Asian dust particles**

338   As seen in Figure 3d, $WSON_p$ presented a monomodal size distribution pattern in

339   Shanghai, peaking at the fine and coarse mode in the NDS and DS periods, respectively. The

340   relative abundance of $WSON_p$ in the coarse mode in the DS period is 0.8 times higher than

341   that in the NDS period. Such an increased $WSON_p$ in the coarse mode in the DS period is in

342   good agreement with that of NACs and IMs and indicates an enhanced formation of

343   nitrogen-containing organic compounds on dust surface (Figure 3b-d).

344   Previous researches have shown that many of nitrogen-containing organic compounds

345   in the troposphere are light absorbing brown carbon (BrC) (Laskin et al., 2015; Liu et al.,

346   2024; Laskin et al., 2025). Thus, here we further investigate the optical properties of the dust

347   samples. As seen in Table 2, Abs_{365} (1.9 M m^{-1}) and MAC_{365} (1.0 m^2 g^{-1}) of BrC in the fine

348   mode during the NDS period were comparable to those during the DS period (2.2 M m^{-1}and

349   0.9 m^2 g^{-1}, respectively). However, Abs_{365} and MAC_{365} (2.6 M m^{-1}, 0.8 m^2 g^{-1}, Table 2) in

350   the coarse mode in the DS period were 2–3 times higher those (0.8 M m^{-1}, 0.4 m^2 g^{-1}, Table

351   2) in the NDS period, respectively, suggesting an enhanced light absorption of coarse

352   particle in the Asian dust storm events. To reveal the nature of such an increase in light

353   absorption of dust particles, we measured the optical properties of atmospheric PM_{10}

354   collected in Tengger Desert. As shown in Figure 4a, MAC of water-soluble BrC in total

355   suspended particles (TSP) in the wavelength range of $\lambda = 250–600$ nm in Shanghai during

356   the DS period is slightly higher than that in the NDS period, but it is more than two times

357   that in Tengger Desert region, suggesting a remarkable increase in light absorption ability of

358   TSP in the downwind city during both NDS and DS periods. MAC_{365} of BrC in the coarse

359   mode during the DS period in Shanghai (0.8 m^2 g^{-1}, Table 2) is four times that in Tengger

360   Desert regions (0.2 ± 0.09 m^2 g^{-1}, Table 2). As shown in Figure 4b, $MAC_{250\text{-}600}$ of water-

361   soluble BrC in the fine mode during both sampling periods were comparable, but the

362    $MAC_{250\text{-}600}$ in the coarse mode during DS period was significantly higher than that in NDS

363   period. Such an increase in light absorption that only occurred in the coarse mode clearly

364   demonstrates that light absorption ability of Asian dust particles in the DS period was

365   significantly strengthened during the long-range transport, which is mostly due to an

366   efficient formation of nitrogen-containing organic compounds on the dust surface.

367   From Figure 4b one may further see that the high $MAC_{250\text{-}600}$ values at the coarse mode

368   in the DS period largely occurred at the 250-350 nm. As reported by previous studies (Yuan

369   et al., 2020; Liu et al., 2023), light absorption of NACs mainly peaks at a wavelength range

370   large than 350 nm while IMs absorb light mostly at a wavelength less than 300 nm. Thus,

371   here we quantified the contribution of IMs light absorption in the coarse mode during DS

372   period. Based on its concentration and light absorption properties, the light absorption

373   contribution of each individual chromophore to the total BrC in the wavelength range of

374   250–400 nm was calculated (Text S2). As seen in Figure 5, IMs show two large absorption

375   peaks at wavelengths of 260 and 290 nm, respectively, which are mainly associated with the

376   absorption of 2IC and 4IC. Moreover, it can also be seen that IMs light absorption

377   contribution to light absorption of water-soluble BrC in DS is almost twice that of NDS,

16

378 indicating a significant contribution of aqueous phase formation to BrC in DS. This result

379 further suggests that an enhanced heterogeneous formation of nitrogen-containing organics

380 including IMs on the dust particles surface are responsible for the increased light absorbing

381 of Asian dust during a long-range transport.   .

382 **4. Summary and implications**

383   In this study we synchronously measured the hourly concentrations of gaseous and

384 particulate WSOC in Shanghai, a downwind city of East Asian desert sources, along with

385 measurements on organic tracers and inorganic ions in the gas- and aerosol- phases. We

386 found that the gas-to-aerosol-phase partitioning coefficient (F_p) of WSOC on the dust storm

387 days (0.3 ± 0.06) in the city is comparable to that on the haze days (0.32 ± 0.06), although

388 the meteorological conditions were drier and hotter during the dust storm period and thus

389 not favorable for the WSOC partitioning, suggesting an enhancing effect of dust particles on

390 the SOA formation on the dust particle surface. In this study, we found the F_p variation was

391 influenced by ALWC in HE but by pH in DS. Moreover, $WSOC_p$ and its light absorption at

392 λ_{365nm} in the coarse mode was increased significantly in DS period than in NDS period.

393 Notably, by comparing with the aerosol optical properties in Tengger desert, we further

394 found that Asian dust aerosols became much more light absorbing with a MAC four times

395 that in the Asian dust source region, which is caused by the enhanced SOA formation on the

396 dust surface during the long-range transport through adsorption and heterogenous formation

397 of light-absorbing brown carbon including nitrogen-containing organics such as

398 nitroaromatics and imidazoles.

399   Atmospheric NACs and IMs are mostly produced from the reactions of aromatic with

400 NO_x in the gas phase and carbonyls with free NH_3 in the aerosol aqueous phase, respectively

401 (Liu et al., 2023; Liu et al., 2024). Although atmospheric SO_2 level in China has been

402 decreased significantly due to strict emission control, the concentrations of NO_x, VOCs and

403 NH_3 in the country are still very high, resulting in SOA in the country much more light

404 absorbing than those in USA and other developed countries (Hecobian et al., 2010; Liu et

405 al., 2024; Li et al., 2025). Our previous studies found that secondary brown carbon is much

406 more favorably formed under a high pH conditions (Liu et al., 2023; Zhang et al., 2024),

407 because (1) nitrophenols are acidic species and thus easier to be adsorbed onto dust surface,

408 and (2) a high pH condition favors NH_4^+ dissociate into $NH_3 + H^+$ and thus can promote the

409 reaction of carbonyl with NH_3.

410 Currently, global aerosol model ensemble estimate that the global dust direct radiative

411 effects is about -0.4 W m^2 (Kok et al., 2017). However, by using an analysis on the size and

412 abundance of dust aerosols to constrain the global model, Abedibi and Kok (2020) found

413 that dust aerosols in the atmosphere is coarser than the size estimated by the current global

414 model ensemble and the dust direct radiative effect is +0.15 W m^2, which means that dust

415 cause a net warming of the planet. Based the results given by this study, we believe that if

416 the secondary formation of light absorbing brown carbon is accounted for the global direct

417 radiative effect of dust aerosol is possibly more warming.

418 **Data Availability.**

419 The data including meteorological data, gaseous pollutants, and major chemical components

420 in $PM_{2.5}$ are freely available at https://doi.org/10.5281/zenodo.14883402 (Li, 2025).

421 **Author Contributions.**

422 GW designed the experiment and supervised the research. ZL, BX, RL and FW collected the

423 samples. ZL, CW, BX, and GW conducted the sample analysis. ZL, BX, CW, RL, and GW

424 performed the data interpretation. ZL, CW and GW wrote the paper. All the authors

425 contributed to the paper with useful scientific discussions.

426 **Competing Interests.**

427 The authors declare no competing financial interest.

428 **Acknowledgement.**

432

References:

Adebiyi, A. A. and Kok, J. F.: Climate models miss most of the coarse dust in the atmosphere, Sci. Adv., 6, https://doi.org/10.1126/sciadv.aaz9507, 2020.

Chen, Q., Miao, R. Q., Geng, G. N., Shrivastava, M., Dao, X., Xu, B. Y., Sun, J. Q., Zhang, X., Liu, M. Y., Tang, G. G., Tang, Q., Hu, H. W., Huang, R. J., Wang, H., Zheng, Y., Qin, Y., Guo, S., Hu, M., and Zhu, T.: Widespread 2013-2020 decreases and reduction challenges of organic aerosol in China, Nat. Commun., 15, https://doi.org/10.1038/s41467-024-48902-0, 2024.

Chen, S., Zhao, D., Huang, J., He, J., Chen, Y., Chen, J., Bi, H., Lou, G., Du, S., Zhang, Y., and Yang, F.: Mongolia Contributed More than 42% of the Dust Concentrations in Northern China in March and April 2023, Adv. Atmos. Sci., 40, 1549-1557, https://doi.org/10.1007/s00376-023-3062-1, 2023.

Cheng, Y., He, K. B., Du, Z. Y., Engling, G., Liu, J. M., Ma, Y. L., Zheng, M., and Weber, R. J.: The characteristics of brown carbon aerosol during winter in Beijing, Atmos. Environ., 127, 355-364, https://doi.org/10.1016/j.atmosenv.2015.12.035, 2016.

El-Sayed, M. M. H., Ortiz-Montalvo, D. L., and Hennigan, C. J.: The effects of isoprene and NOx on secondary organic aerosols formed through reversible and irreversible uptake to aerosol water, Atmos. Chem. Phys., 18, 1171-1184, https://doi.org/10.5194/acp-18-1171-2018, 2018.

Ervens, B., Turpin, B. J., and Weber, R. J.: Secondary organic aerosol formation in cloud droplets and aqueous particles (aqSOA): a review of laboratory, field and model studies, Atmos. Chem. Phys., 11, 11069-11102, https://doi.org/10.5194/acp-11-11069-2011, 2011.

Fountoukis, C. and Nenes, A.: ISORROPIA II: a computationally efficient thermodynamic equilibrium model for K+-Ca2+-Mg2+-NH4+-Na+-SO42--NO3--Cl--H2O aerosols, Atmos. Chem. Phys., 7, 4639-4659, https://doi.org/10.5194/acp-7-4639-2007, 2007.

Ge, J., Li, W., Huang, J., Mu, Q., Li, Q., Zhao, Q., Su, J., Xie, Y., Alam, K., Zhu, Z., and Hu, X.: Dust Accelerates the Life Cycle of High Clouds Unveiled Through Strongly-Constrained Meteorology, Geophys. Res. Lett., 51, e2024GL109998, https://doi.org/10.1029/2024GL109998, 2024.

Gkatzelis, G. I., Papanastasiou, D. K., Karydis, V. A., Hohaus, T., Liu, Y., Schmitt, S. H., Schlag, P., Fuchs, H., Novelli, A., Chen, Q., Cheng, X., Broch, S., Dong, H., Holland, F., Li, X., Liu, Y., Ma, X., Reimer, D., Rohrer, F., Shao, M., Tan, Z., Taraborrelli, D., Tillmann, R., Wang, H., Wang, Y., Wu, Y., Wu, Z., Zeng, L., Zheng, J., Hu, M., Lu, K., Hofzumahaus, A., Zhang, Y., Wahner, A., and Kiendler-Scharr, A.: Uptake of Water-soluble Gas-phase Oxidation Products Drives Organic Particulate Pollution in Beijing, Geophys. Res. Lett., 48, e2020GL091351, https://doi.org/10.1029/2020GL091351, 2021.

Hecobian, A., Zhang, X., Zheng, M., Frank, N., Edgerton, E. S., and Weber, R. J.: Water-Soluble Organic Aerosol material and the light-absorption characteristics of aqueous extracts measured

over the Southeastern United States, Atmos. Chem. Phys., 10, 5965-5977,
https://doi.org/10.5194/acp-10-5965-2010, 2010.

Hems, R. F., Schnitzler, E. G., Bastawrous, M., Soong, R., Simpson, A. J., and Abbatt, J. P. D.:
Aqueous Photoreactions of Wood Smoke Brown Carbon, ACS Earth Space Chem., 4, 1149-1160,
https://doi.org/10.1021/acsearthspacechem.0c00117, 2020.

Hennigan, C. J., Bergin, M. H., Russell, A. G., Nenes, A., and Weber, R. J.: Gas/particle partitioning
of water-soluble organic aerosol in Atlanta, Atmos. Chem. Phys., 9, 3613-3628,
https://doi.org/10.5194/acp-9-3613-2009, 2009.

Huang, R.-J., Zhang, Y., Bozzetti, C., Ho, K.-F., Cao, J.-J., Han, Y., Daellenbach, K. R., Slowik, J.
G., Platt, S. M., Canonaco, F., Zotter, P., Wolf, R., Pieber, S. M., Bruns, E. A., Crippa, M.,
Ciarelli, G., Piazzalunga, A., Schwikowski, M., Abbaszade, G., Schnelle-Kreis, J., Zimmermann,
R., An, Z., Szidat, S., Baltensperger, U., Haddad, I. E., and Prévôt, A. S. H.: High secondary
aerosol contribution to particulate pollution during haze events in China, Nature, 514, 218-222,
https://doi.org/10.1038/nature13774, 2014.

Kok, J. F., Ridley, D. A., Zhou, Q., Miller, R. L., Zhao, C., Heald, C. L., Ward, D. S., Albani, S., and
Haustein, K.: Smaller desert dust cooling effect estimated from analysis of dust size and
abundance, Nat. Geosci., 10, 274-278, https://doi.org/10.1038/Ngeo2912, 2017.

Laskin, A., Laskin, J., and Nizkorodov, S. A.: Chemistry of Atmospheric Brown Carbon, Chem.
Rev., 115, 4335-4382, https://doi.org/10.1021/cr5006167, 2015.

Laskin, A., West, C. P., and Hettiyadura, A. P. S.: Molecular insights into the composition, sources,
and aging of atmospheric brown carbon, Chem Soc Rev, 54, 1583-1612,
https://doi.org/10.1039/d3cs00609c, 2025.

Laskin, A., Wietsma, T. W., Krueger, B. J., and Grassian, V. H.: Heterogeneous chemistry of
individual mineral dust particles with nitric acid: A combined CCSEM/EDX, ESEM, and ICP-
MS study, J. Geophys. Res-Atmos., 110, https://doi.org/10.1029/2004JD005206, 2005.

Lauraguais, A., Coeur-Tourneur, C., Cassez, A., Deboudt, K., Fourmentin, M., and Choël, M.:
Atmospheric reactivity of hydroxyl radicals with guaiacol (2-methoxyphenol), a biomass burning
emitted compound: Secondary organic aerosol formation and gas-phase oxidation products,
Atmos. Environ., 86, 155-163, https://doi.org/10.1016/j.atmosenv.2013.11.074, 2014.

Li, D. P., Wu, C., Zhang, S., Lei, Y. L., Lv, S. J., Du, W., Liu, S. J., Zhang, F., Liu, X. D., Liu, L.,
Meng, J. J., Wang, Y. S., Gao, J., and Wang, G. H.: Significant coal combustion contribution to
water-soluble brown carbon during winter in Xingtai, China: Optical properties and sources, J.
Environ. Sci., 124, 892-900, https://doi.org/10.1016/j.jes.2022.02.026, 2023a.

Li, H., Qin, X., Chen, J., Wang, G., Liu, C., Lu, D., Zheng, H., Song, X., Gao, Q., Xu, J., Zhu, Y.,
Liu, J., Wang, X., Deng, C., and Huang, K.: Continuous Measurement and Molecular
Compositions of Atmospheric Water-Soluble Brown Carbon in the Nearshore Marine Boundary

Layer of Northern China: Secondary Formation and Influencing Factors, J. Geophys. Res-Atmos., 128, e2023JD038565, https://doi.org/10.1029/2023JD038565, 2023b.

Li, J. J., Li, J., Wang, G. H., Zhang, T., Dai, W. T., Ho, K. F., Wang, Q. Y., Shao, Y., Wu, C., and Li, L.: Molecular characteristics of organic compositions in fresh and aged biomass burning aerosols, Sci. Total Environ., 741, https://doi.org/10.1016/j.scitotenv.2020.140247, 2020.

Li, R., Cui, L., Zhao, Y., Zhou, W., and Fu, H.: Long-term trends of ambient nitrate (NO_3^-) concentrations across China based on ensemble machine-learning models, Earth Syst. Sci. Data, 13, 2147-2163, 10.5194/essd-13-2147-2021, 2021.

Li, W., Shao, L., Shi, Z., Chen, J., Yang, L., Yuan, Q., Yan, C., Zhang, X., Wang, Y., Sun, J., Zhang, Y., Shen, X., Wang, Z., and Wang, W.: Mixing state and hygroscopicity of dust and haze particles before leaving Asian continent, J. Geophys. Res-Atmos., 119, 1044-1059, https://doi.org/10.1002/2013JD021003, 2014.

Li, W. J. and Shao, L. Y.: Observation of nitrate coatings on atmospheric mineral dust particles, Atmos. Chem. Phys., 9, 1863-1871, https://doi.org/10.5194/acp-9-1863-2009, 2009.

Li, Y., Fu, T.-M., Yu, J. Z., Zhang, A., Yu, X., Ye, J., Zhu, L., Shen, H., Wang, C., Yang, X., Tao, S., Chen, Q., Li, Y., Li, L., Che, H., and Heald, C. L.: Nitrogen dominates global atmospheric organic aerosol absorption, Science, 387, 989-995, https://doi.org/10.1126/science.adr4473, 2025.

Lian, X., Zhang, G., Yang, Y., Lin, Q., Fu, Y., Jiang, F., Peng, L., Hu, X., Chen, D., Wang, X., Peng, P. a., Sheng, G., and Bi, X.: Evidence for the Formation of Imidazole from Carbonyls and Reduced Nitrogen Species at the Individual Particle Level in the Ambient Atmosphere, Environ. Sci. Tech. Let., 8, 9-15, https://doi.org/10.1021/acs.estlett.0c00722, 2021.

Liang, Y. H., Wang, X. F., Dong, S. W., Liu, Z. Y., Mu, J. S., Lu, C. Y., Zhang, J., Li, M., Xue, L. K., and Wang, W. X.: Size distributions of nitrated phenols in winter at a coastal site in north China and the impacts from primary sources and secondary formation, Chemosphere, 250, https://doi.org/10.1016/j.chemosphere.2020.126256, 2020.

Liu, J., Zhang, X., Parker, E. T., Veres, P. R., Roberts, J. M., de Gouw, J. A., Hayes, P. L., Jimenez, J. L., Murphy, J. G., Ellis, R. A., Huey, L. G., and Weber, R. J.: On the gas-particle partitioning of soluble organic aerosol in two urban atmospheres with contrasting emissions: 2. Gas and particle phase formic acid, J. Geophys. Res-Atmos., 117, https://doi.org/10.1029/2012JD017912, 2012.

Liu, S., Huang, D., Wang, Y., Zhang, S., Liu, X., Wu, C., Du, W., and Wang, G.: Synergetic effects of NH_3 and NO_x on the production and optical absorption of secondary organic aerosol formation from toluene photooxidation, Atmos. Chem. Phys., 21, 17759-17773, https://doi.org/10.5194/acp-21-17759-2021, 2021.

Liu, X., Wang, H., Wang, F., Lv, S., Wu, C., Zhao, Y., Zhang, S., Liu, S., Xu, X., Lei, Y., and Wang, G.: Secondary Formation of Atmospheric Brown Carbon in China Haze: Implication for an

541   Enhancing Role of Ammonia, Environ. Sci. Technol., 57, 11163-11172,

542   https://doi.org/10.1021/acs.est.3c03948, 2023.

543   Liu, X., Wu, C., Li, Z., Li, R., Wang, F., Lv, S., Li, R., Zhang, F., Wang, H., Liang, C., Zhang, L., and

544   Wang, G.: Atmospheric brown carbon in China haze is dominated by secondary formation, Sci.

545   Total Environ., 945, 173901, https://doi.org/10.1016/j.scitotenv.2024.173901, 2024.

546   Liu, Y. C., Zhan, J. L., Zheng, F. X., Song, B. Y., Zhang, Y. S., Ma, W., Hua, C. J., Xie, J. L., Bao, X.

547   L., Yan, C., Bianchi, F., Petäjä, T., Ding, A. J., Song, Y., He, H., and Kulmala, M.: Dust emission

548   reduction enhanced gas-to-particle conversion of ammonia in the North China Plain, Nat.

549   Commun., 13, https://doi.org/10.1038/s41467-022-34733-4, 2022.

550   Lutz, A., Mohr, C., Le Breton, M., Lopez-Hilfiker, F. D., Priestley, M., Thornton, J. A., and

551   Hallquist, M.: Gas to Particle Partitioning of Organic Acids in the Boreal Atmosphere, ACS Earth

552   Space Chem., 3, 1279-1287, http://doi.org/10.1021/acsearthspacechem.9b00041, 2019.

553   Lv, S. J., Wu, C., Wang, F. L., Liu, X. D., Zhang, S., Chen, Y. B., Zhang, F., Yang, Y., Wang, H. L.,

554   Huang, C., Fu, Q. Y., Duan, Y. S., and Wang, G. H.: Nitrate-Enhanced Gas-to-Particle-Phase

555   Partitioning of Water- Soluble Organic Compounds in Chinese Urban Atmosphere: Implications

556   for Secondary Organic Aerosol Formation, Environ. Sci. Tech. Let., 10, 14-20,

557   https://doi.org/10.1021/acs.estlett.2c00894, 2022a.

558   Lv, S. J., Wang, F. L., Wu, C., Chen, Y. B., Liu, S. J., Zhang, S., Li, D. P., Du, W., Zhang, F., Wang,

559   H. L., Huang, C., Fu, Q. Y., Duan, Y. S., and Wang, G. H.: Gas-to-Aerosol Phase Partitioning of

560   Atmospheric Water-Soluble Organic Compounds at a Rural Site in China: An Enhancing Effect

561   of NH3 on SOA Formation, Environ. Sci. Technol., 56, 3915-3924,

562   https://doi.org/10.1021/acs.est.1c06855, 2022b.

563   Na, K., Song, C., Switzer, C., and Cocker, D. R.: Effect of Ammonia on Secondary Organic Aerosol

564   Formation from α-Pinene Ozonolysis in Dry and Humid Conditions, Environ. Sci. Technol., 41,

565   6096-6102, https://doi.org/10.1021/es061956y, 2007.

566   Pankow, J. F.: An absorption model of the gas/aerosol partitioning involved in the formation of

567   secondary organic aerosol, Atmos. Environ., 28, 189-193, https://doi.org/10.1016/1352-

568   2310(94)90094-9, 1994.

569   Ren, Y., Wang, G., Wei, J., Tao, J., Zhang, Z., and Li, H.: Contributions of primary emissions and

570   secondary formation to nitrated aromatic compounds in themountain background region of

571   Southeast China, Atmos. Chem. Phys., 23, 6835-6848, https://doi.org/10.5194/acp-23-6835-

572   2023, 2023.

573   Song, S., Gao, M., Xu, W., Shao, J., Shi, G., Wang, S., Wang, Y., Sun, Y., and McElroy, M. B.: Fine-

574   particle pH for Beijing winter haze as inferred from different thermodynamic equilibrium

575   models, Atmos. Chem. Phys., 18, 7423-7438, https://doi.org/10.5194/acp-18-7423-2018, 2018.

576   Tang, M., Cziczo, D. J., and Grassian, V. H.: Interactions of Water with Mineral Dust Aerosol: Water

577   Adsorption, Hygroscopicity, Cloud Condensation, and Ice Nucleation, Chem. Rev., 116, 4205-
578   4259, https://doi.org/10.1021/acs.chemrev.5b00529, 2016.

579 Tang, M., Guo, L., Bai, Y., Huang, R.-J., Wu, Z., Wang, Z., Zhang, G., Ding, X., Hu, M., and Wang,
580   X.: Impacts of methanesulfonate on the cloud condensation nucleation activity of sea salt aerosol,
581   Atmos. Environ., 201, 13-17, https://doi.org/10.1016/j.atmosenv.2018.12.034, 2019.

582 Tobo, Y., Zhang, D., Matsuki, A., and Iwasaka, Y.: Asian dust particles converted into aqueous
583   droplets under remote marine atmospheric conditions, P. Natl. Acad. Sci. U.S.A., 107, 17905-
584   17910, https://doi.org/10.1073/pnas.1008235107, 2010.

585 Vione, D., Maurino, V., Minero, C., Lucchiari, M., and Pelizzetti, E.: Nitration and hydroxylation of
586   benzene in the presence of nitrite/nitrous acid in aqueous solution, Chemosphere, 56, 1049-1059,
587   https://doi.org/10.1016/j.chemosphere.2004.05.027, 2004.

588 Wang, G., Zhang, S., Wu, C., Zhu, T., Xu, X., Ge, S., Sun, H., Sun, Z., Wang, J., Ji, Y., Gao, J., Ren,
589   Y., Li, H., Zhang, F., Wang, Y., and Seinfeld, J. H.: Atmospheric sulfate aerosol formation
590   enhanced by interfacial anions, PNAS Nexus, 4, pgaf058,
591   http://doi.org/10.1093/pnasnexus/pgaf058, 2025.

592 Wang, G., Zhang, R., Gomez, M. E., Yang, L., Levy Zamora, M., Hu, M., Lin, Y., Peng, J., Guo, S.,
593   Meng, J., Li, J., Cheng, C., Hu, T., Ren, Y., Wang, Y., Gao, J., Cao, J., An, Z., Zhou, W., Li, G.,
594   Wang, J., Tian, P., Marrero-Ortiz, W., Secrest, J., Du, Z., Zheng, J., Shang, D., Zeng, L., Shao,
595   M., Wang, W., Huang, Y., Wang, Y., Zhu, Y., Li, Y., Hu, J., Pan, B., Cai, L., Cheng, Y., Ji, Y.,
596   Zhang, F., Rosenfeld, D., Liss, P. S., Duce, R. A., Kolb, C. E., and Molina, M. J.: Persistent
597   sulfate formation from London Fog to Chinese haze, P. Natl. Acad. Sci. U.S.A., 113, 13630,
598   https://doi.org/10.1073/pnas.1616540113, 2016.

599 Wang, G. H., Kawamura, K., and Lee, M.: Comparison of organic compositions in dust storm and
600   normal aerosol samples collected at Gosan, Jeju Island, during spring 2005, Atmos. Environ., 43,
601   219-227, http://doi.org/10.1016/j.atmosenv.2008.09.046, 2009.

602 Wang, G. H., Cheng, C. L., Meng, J. J., Huang, Y., Li, J. J., and Ren, Y. Q.: Field observation on
603   secondary organic aerosols during Asian dust storm periods: Formation mechanism of oxalic acid
604   and related compounds on dust surface, Atmos. Environ., 113, 169-176,
605   http://doi.org/10.1016/j.atmosenv.2015.05.013, 2015.

606 Wang, G. H., Kawamura, K., Cheng, C. L., Li, J. J., Cao, J. J., Zhang, R. J., Zhang, T., Liu, S. X.,
607   and Zhao, Z. Z.: Molecular Distribution and Stable Carbon Isotopic Composition of Dicarboxylic
608   Acids, Ketocarboxylic Acids, and α-Dicarbonyls in Size-Resolved Atmospheric Particles From
609   Xi'an City, China, Environ. Sci. Technol., 46, 4783-4791, https://doi.org/10.1021/es204322c,
610   2012.

611 Wang, G. H., Cheng, C. L., Huang, Y., Tao, J., Ren, Y. Q., Wu, F., Meng, J. J., Li, J. J., Cheng, Y. T.,
612   Cao, J. J., Liu, S. X., Zhang, T., Zhang, R., and Chen, Y. B.: Evolution of aerosol chemistry in

Xi'an, inland China, during the dust storm period of 2013-Part 1: Sources, chemical forms and formation mechanisms of nitrate and sulfate, Atmos. Chem. Phys., 14, 11571-11585, https://doi.org/10.5194/acp-14-11571-2014, 2014.

Wang, G. H., Zhang, F., Peng, J. F., Duan, L., Ji, Y. M., Marrero-Ortiz, W., Wang, J. Y., Li, J. J., Wu, C., Cao, C., Wang, Y., Zheng, J., Secrest, J., Li, Y. X., Wang, Y. Y., Li, H., Li, N., and Zhang, R. Y.: Particle acidity and sulfate production during severe haze events in China cannot be reliably inferred by assuming a mixture of inorganic salts, Atmos. Chem. Phys., 18, 10123-10132, https://doi.org/10.5194/acp-18-10123-2018, 2018.

Wang, H. C., Wang, H. L., Lu, X., Lu, K. D., Zhang, L., Tham, Y. J., Shi, Z. B., Aikin, K., Fan, S. J., Brown, S. S., and Zhang, Y. H.: Increased night-time oxidation over China despite widespread decrease across the globe, Nat. Geosci., 16, 217-+, https://doi.org/10.1038/s41561-022-01122-x, 2023.

Wang, Y., Hu, M., Wang, Y., Zheng, J., Shang, D., Yang, Y., Liu, Y., Li, X., Tang, R., Zhu, W., Du, Z., Wu, Y., Guo, S., Wu, Z., Lou, S., Hallquist, M., and Yu, J. Z.: The formation of nitro-aromatic compounds under high NOx and anthropogenic VOC conditions in urban Beijing, China, Atmos. Chem. Phys., 19, 7649-7665, http://doi.org/10.5194/acp-19-7649-2019, 2019.

Wang, Z. L., Huang, X., Wang, N., Xu, J. W., and Ding, A. J.: Aerosol-Radiation Interactions of Dust Storm Deteriorate Particle and Ozone Pollution in East China, J. Geophys. Res-Atmos., 125, https://doi.org/10.1029/2020JD033601, 2020.

Wu, C., Zhang, S., Wang, G. H., Lv, S. J., Li, D. P., Liu, L., Li, J. J., Liu, S. J., Du, W., Meng, J. J., Qiao, L. P., Zhou, M., Huang, C., and Wang, H. L.: Efficient Heterogeneous Formation of Ammonium Nitrate on the Saline Mineral Particle Surface in the Atmosphere of East Asia during Dust Storm Periods, Environ. Sci. Technol., 54, 15622-15630, https://doi.org/10.1021/acs.est.0c04544, 2020.

Xiao, Q. Y., Geng, G. N., Xue, T., Liu, S. G., Cai, C. L., He, K. B., and Zhang, Q.: Tracking PM2.5 and O3 Pollution and the Related Health Burden in China 2013-2020, Environ. Sci. Technol., 56, 6922-6932, https://doi.org/10.1021/acs.est.1c04548, 2022.

Yuan, W., Huang, R. J., Yang, L., Guo, J., Chen, Z., Duan, J., Wang, T., Ni, H., Han, Y., Li, Y., Chen, Q., Chen, Y., Hoffmann, T., and O'Dowd, C.: Characterization of the light-absorbing properties, chromophore composition and sources of brown carbon aerosol in Xi'an, northwestern China, Atmos. Chem. Phys., 20, 5129-5144, https://doi.org/10.5194/acp-20-5129-2020, 2020.

Zhang, F., Wang, Y., Peng, J. F., Chen, L., Sun, Y. L., Duan, L., Ge, X. L., Li, Y. X., Zhao, J. Y., Liu, C., Zhang, X. C., Zhang, G., Pan, Y. P., Wang, Y. S., Zhang, A. L., Ji, Y. M., Wang, G. H., Hu, M., Molina, M. J., and Zhang, R. Y.: An unexpected catalyst dominates formation and radiative forcing of regional haze, P. Natl. Acad. Sci. U.S.A., 117, 3960-3966, https://doi.org/10.1073/pnas.1919343117, 2020.

649   Zhang, R., Wang, G., Guo, S., Zamora, M. L., Ying, Q., Lin, Y., Wang, W., Hu, M., and Wang, Y.:

650   Formation of Urban Fine Particulate Matter, Chem. Rev., 115, 3803-3855,

651   https://doi.org/10.1021/acs.chemrev.5b00067, 2015.

652   Zhang, S., Gao, Y. N., Xu, X. B., Chen, L. Y., Wu, C., Li, Z., Li, R. J., Xiao, B. Y., Liu, X. D., Li, R.,

653   Zhang, F., and Wang, G. H.: Heterogeneous formation and light absorption of secondary organic

654   aerosols from acetone photochemical reactions: remarkably enhancing effects of seeds and

655   ammonia, Atmos. Chem. Phys., 24, 14177-14190, https://doi.org/10.5194/acp-24-14177-2024,

656   2024.

657   Zhang, X., Liu, J., Parker, E. T., Hayes, P. L., Jimenez, J. L., de Gouw, J. A., Flynn, J. H., Grossberg,

658   N., Lefer, B. L., and Weber, R. J.: On the gas-particle partitioning of soluble organic aerosol in

659   two urban atmospheres with contrasting emissions: 1. Bulk water-soluble organic carbon, J.

660   Geophys. Res-Atmos., 117, https://doi.org/doi.org/10.1029/2012JD017908, 2012.

661

662 **Table 1**. Meteorological parameters and concentrations of gaseous and particulate pollutants

663 in PM$_{2.5}$ in Shanghai during the spring 2023 campaign

	Whole campaign	Dust storm	Haze event	Clean period
I Meteorological parameters and gaseous pollutants				
RH (%)	59 ± 14	44 ± 18	61 ± 13	63 ± 9
T (°C)	17 ± 4	17 ± 3	13 ± 3	21 ± 3
WSOC$_g$[a] (µgC m^{-3})	8.0 ± 3.4	6.1 ± 1.5	6.0 ± 1.4	8.2 ± 3.3
II Major components of PM$_{2.5}$				
PM$_{2.5}$ (µg m^{-3})	30 ± 14	39 ± 16	43 ± 16	20 ± 7
PM$_{10}$ (µg m^{-3})	76 ± 89	301 ± 192	58 ± 15	43 ± 19
WSOC$_p$[a] (µgC m^{-3})	3.1 ± 1.3	2.6 ± 0.7	3.0 ± 0.8	2.8 ± 1.7
NH$_4^+$ (µg m^{-3})	3.7 ± 2.5	1.3 ± 1.3	6.8 ± 2.1	2.2 ± 0.9
NO$_3^-$ (µg m^{-3})	7.7 ± 6.5	3.2 ± 2.5	15.2 ± 6.2	2.9 ± 1.5
SO$_4^{2-}$ (µg m^{-3})	4.2 ± 2.6	2.1 ± 2.2	6.8 ± 2.9	3.7 ± 1.8
SNA (µg m^{-3})[b]	13.3 ± 11.1	6.5 ± 5.6	25.6 ± 13.1	8.5 ± 3.9
SNA/PM$_{2.5}$ (%)[c]	55 ± 22	16 ± 12	68 ± 13	44 ± 12
Ca^{2+} (µg m^{-3})	0.1 ± 0.2	0.6 ± 0.5	0.08 ± 0.05	0.01 ± 0.01
ALWC[c] (µg m^{-3})[d]	9.6 ± 12.1	2.7 ± 2.2	18.5 ± 14.4	5.3 ± 2.5
pH of PM$_{2.5}$	3.4 ± 0.8	4.8 ± 1.5	3.4 ± 0.3	2.8 ± 0.5
F$_p$[f]	0.28 ± 0.08	0.3 ± 0.06	0.32 ± 0.06	0.24 ± 0.06

664 [a]WSOC$_g$, is the gas-phase organics while WSOC$_p$, is the organics in PM$_{2.5}$. [b]SNA is the sum of sulfate,

665 nitrate and ammonium. [c]Ratio of sum of NH$_4^+$, NO$_3^-$ and SO$_4^{2-}$ to PM$_{2.5}$. [d]ALWC: aerosol liquid water

666 content of PM$_{2.5}$. [f]$F_p = \dfrac{WSOC_p}{WSOC_g + WSOC_p}$

667 **Table 2**. Concentrations of WSOC$_p$, WSON$_p$, organic acids, and inorganic ions and optical

668 properties of WSOC$_p$ in airborne particles in Shanghai and Tengger Desert region

	Non-dust storm		Dust storm		Tengger Desert
	Fine mode (<2.1μm)	Coarse mode (>2.1μm)	Fine mode (<2.1μm)	Coarse mode (>2.1μm)	PM$_{10}$
WSOC$_p$ (μgC m^{-3})	2.0 ± 0.02	1.8 ± 0.02	2.4 ± 0.01	3.4 ± 0.01	14 ± 7.5
WSON$_p$ (μgN m^{-3})	1.1 ± 0.02	0.3 ± 0.01	0.7 ± 0.01	0.5 ± 0.01	ND[c]
PM (μg m^{-3})	19	48	52	367	402 ± 75
Oxalic acid (μg m^{-3})	0.7 ± 0.04	0.4 ± 0.02	0.3 ± 0.02	1.4 ± 0.1	0.7 ± 0.08
Pyr[a] (μg m^{-3})	0.06 ± 0.01	0.09 ± 0.01	0.03 ± 0.01	0.2 ± 0.01	0.03 ± 0.01
MSA[b] (μg m^{-3})	0.1 ± 0.01	0.1± 0.02	0.09 ± 0.01	0.5 ± 0.04	ND[c]
NACs (ng m^{-3})	0.5± 0.02	0.9 ± 0.03	0.5 ± 0.01	1.7 ± 0.01	ND[c]
IMs (ng m^{-3})	0.7 ± 0.02	0.1 ± 0.01	0.5 ± 0.02	0.2 ± 0.01	ND[c]
Abs$_{365}$ (M m^{-1})	1.9 ± 0.2	0.8 ± 0.08	2.2 ± 0.2	2.6 ± 0.3	2.5 ± 0.4
MAC$_{365}$ (m^2 g^{-1})	1.0 ± 0.04	0.4 ± 0.02	0.9 ± 0.04	0.8 ± 0.04	0.2 ± 0.09

669 [a] Pyr: pyruvic acid. [b] MSA: methanesulfonic acid. [c]ND: Not Detected

670

Figure Caption

Figure 1. Temporal variations in meteorological parameters and concentrations of major components in $PM_{2.5}$ during the spring of 2023 in Shanghai, China.
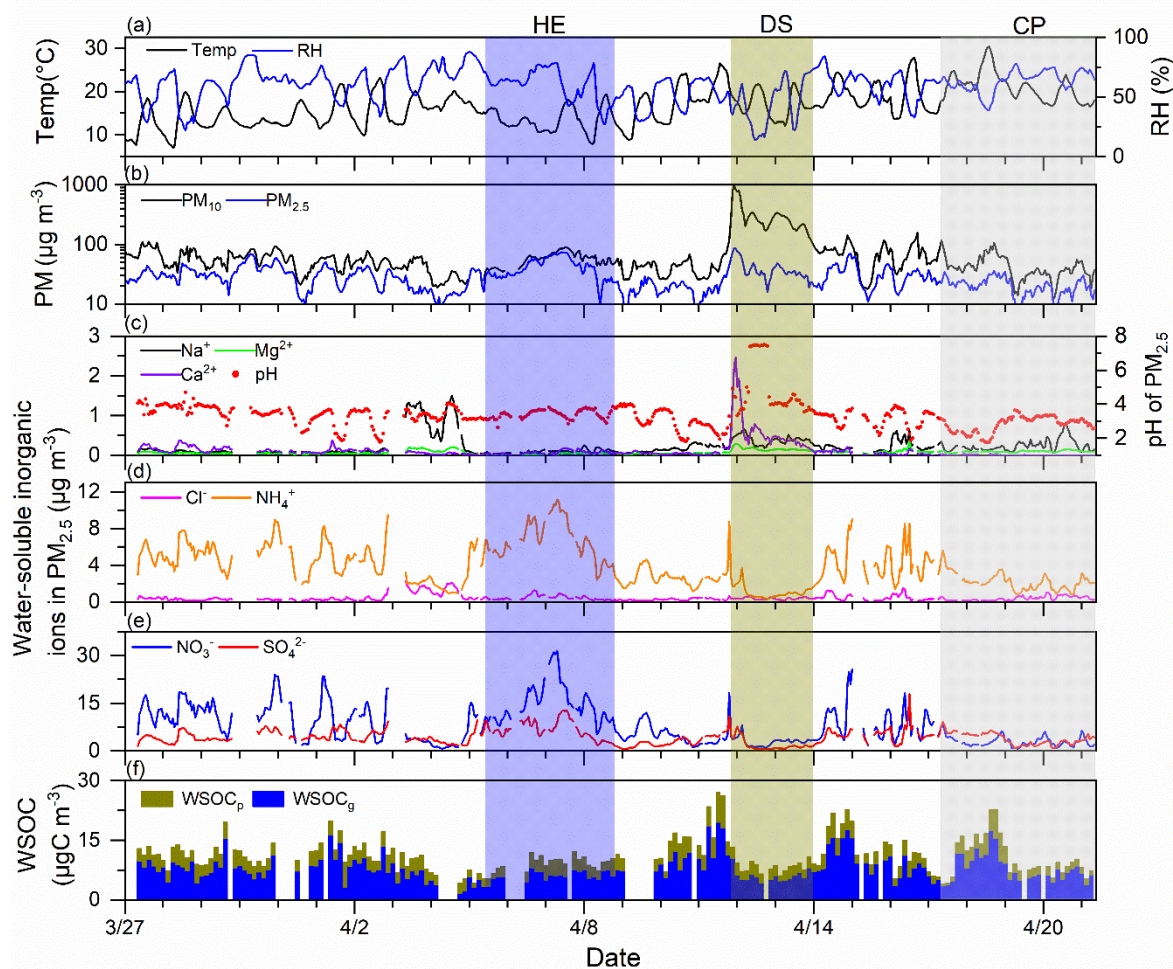
Figure 2. Factors controlling the gas-to-particle phase partitioning of WSOC in haze (HE) and dust storm (DS) events. (a) F_p as a function of ALWC in HE and DS. (b) ALWC as a function of ammonia partitioning coefficient ($\varepsilon(NH_4^+) = NH_4^+ / (NH_3 + NH_4^+)$) in HE. (c) Dependence of $WSOC_p$ concentrations on ALWC in HE. (d) Linear regression fit for TNH_x versus $WSOC_p$ concentration during HE and DS periods. (e) F_p of WSOCs as a function of pH during HE and DS periods. (f) Linear regression fit for particulate organic acids and metal cations in HE and DS periods.

Figure 3. Size distributions of $WSOC_p$, $WSON_p$, nitro-aromatic compounds (NACs) and imidazoles (IMs) in Shanghai during the non-dust storm (NDS) and dust storm (DS) periods.

Figure 4. Optical properties of $WSOC_p$ of PM_{10} in Tengger Desert regions and TSP in Shanghai during the dust storm (DS) and non-dust storm (DS) periods. (a) Mass absorption coefficient (MAC) of $WSOC_p$. (b) MAC of $WSOC_p$ in the fine ($<2.1\mu m$) and coarse ($>2.1\mu m$) modes of atmospheric particles in Shanghai.
.

Figure 5. Light absorption contributions of IMs to water-soluble BrC over the wavelength range of 250-400 nm in the coarse mode in NDS and DS periods.

696

697

Figure 1. Temporal variations in meteorological parameters and concentrations of major

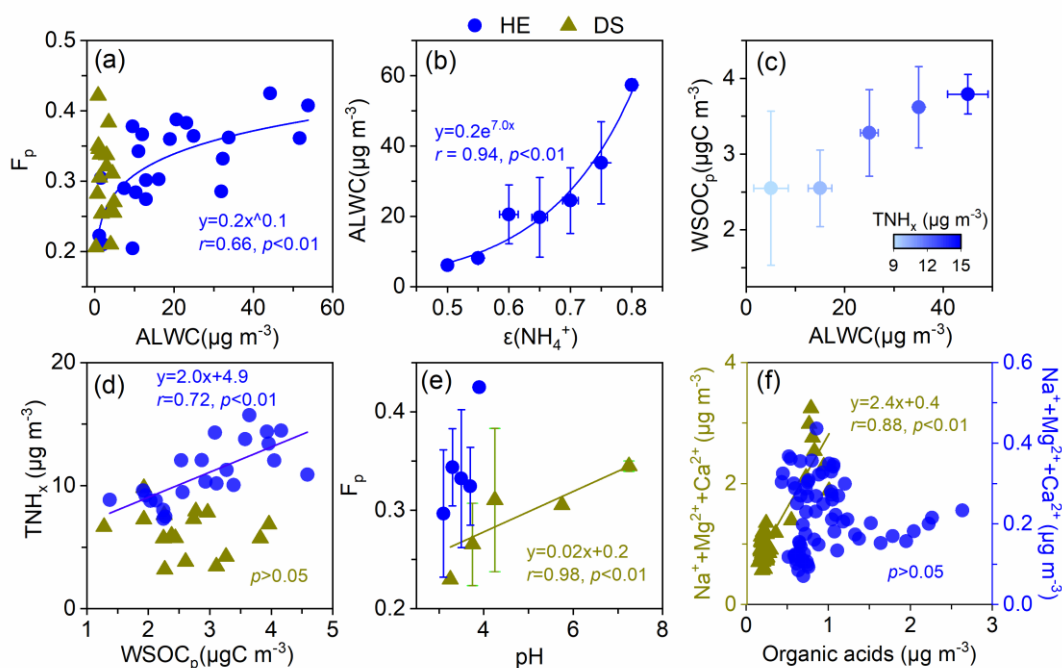components in PM$_{2.5}$ during the spring of 2023 in Shanghai, China.

700

701

Figure 2. Factors controlling the gas-to-particle phase partitioning of WSOC in haze (HE) and dust storm (DS) events. (a) F_p as a function of ALWC in HE and DS. (b) ALWC as a function of ammonia partitioning coefficient ($\varepsilon(NH_4^+) = NH_4^+ / (NH_3 + NH_4^+)$) in HE. (c) Dependence of $WSOC_p$ concentrations on ALWC in HE. (d) Linear regression fit for TNH_x versus $WSOC_p$ concentration during HE and DS periods. (e) F_p of WSOCs as a function of pH during HE and DS periods. (f) Linear regression fit for particulate organic acids and metal cations in HE and DS periods.
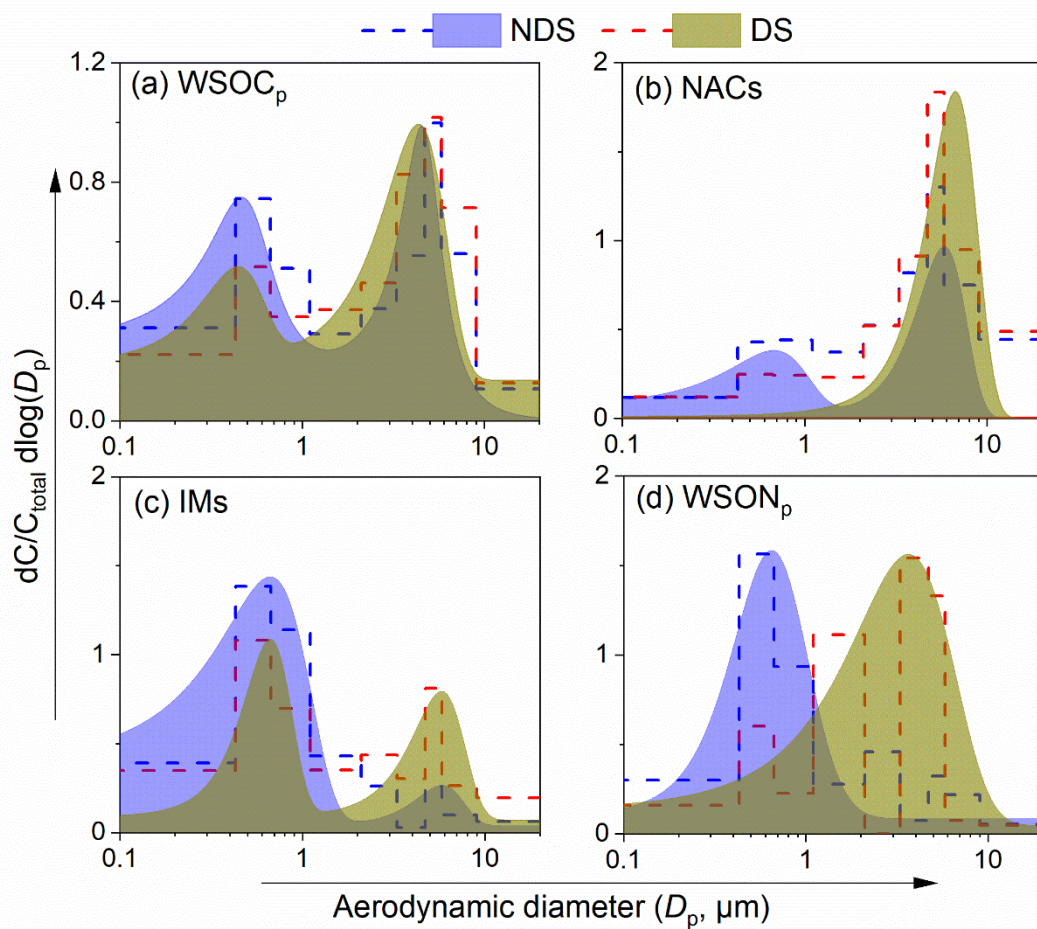
Figure 3. Size distributions of $WSOC_p$, $WSON_p$, nitro-aromatic compounds (NACs) and imidazoles (IMs) in Shanghai during the non-dust storm (NDS) and dust storm (DS) periods. The dashed lines and filled areas are the measured size distribution and fitting results, respectively (C_{total} is the sum of concentration on all the 9-stages).
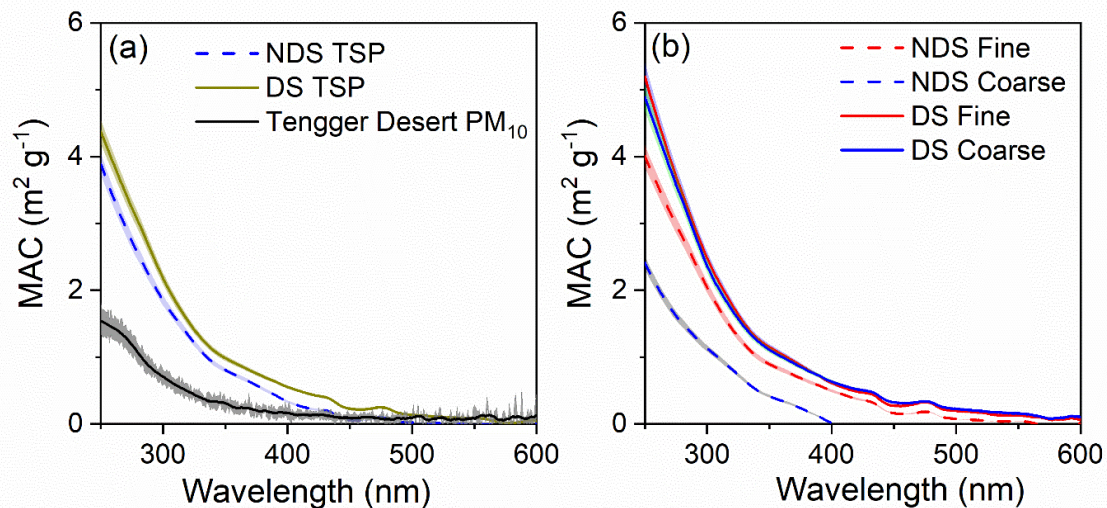
Figure 4. Optical properties of $WSOC_p$ of PM_{10} in Tengger Desert regions and TSP in Shanghai during the dust storm (DS) and non-dust storm (DS) periods. (a) Mass absorption coefficient (MAC) of $WSOC_p$. (b) MAC of $WSOC_p$ in the fine ($<2.1\mu m$) and coarse ($>2.1\mu m$) modes of atmospheric particles in Shanghai.
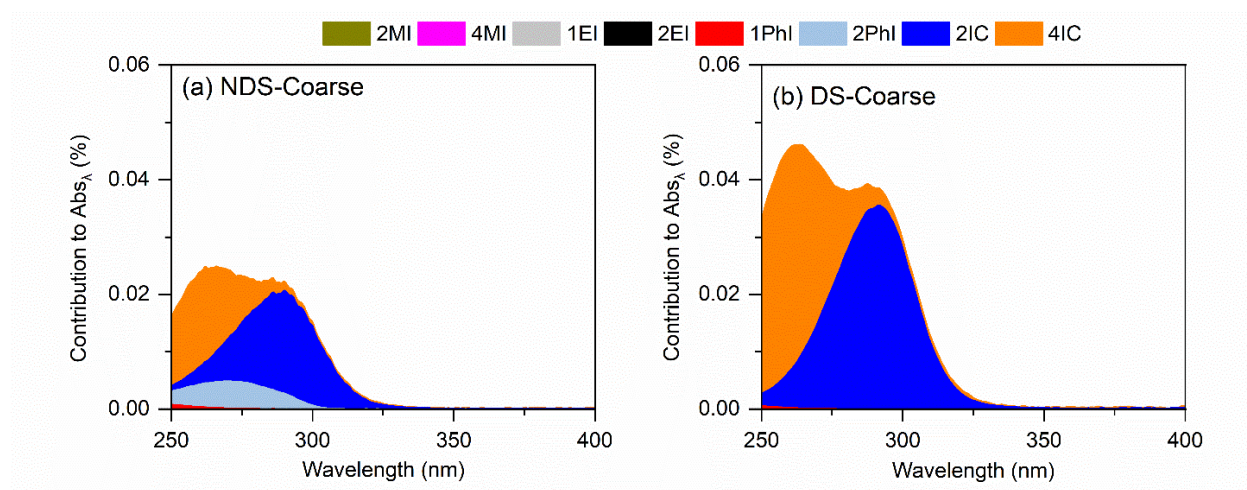
Figure 5. Light absorption contributions of IMs to water-soluble BrC over the wavelength range of 250-400 nm in the coarse mode in NDS and DS periods.